

CrossMark  
click for updatesCite this: *RSC Adv.*, 2016, 6, 62705

# Adsorption mechanism on metal organic frameworks of Cu-BTC, Fe-BTC and ZIF-8 for CO<sub>2</sub> capture investigated by X-ray absorption fine structure

Meng Du,<sup>ab</sup> Lina Li,<sup>\*b</sup> Mingxing Li<sup>a</sup> and Rui Si<sup>b</sup>

Three different commercial metal–organic frameworks (MOFs) of Cu-BTC, Fe-BTC and ZIF-8 have been characterized by multiple techniques including CO<sub>2</sub> adsorption/desorption, scanning electron microscopy (SEM), transmission electron microscopy (TEM), X-ray diffraction (XRD) and X-ray absorption fine structure (XAFS). Particularly, the MOFs powders were sealed inside quartz sample tubes for each step of CO<sub>2</sub> adsorption/desorption, and were sequentially measured for XAFS to identify the short-range structural evolutions on investigated metals (Cu, Fe, Zn). According to the data analyses on X-ray absorption near edge spectroscopy (XANES) and extended X-ray absorption fine structure (EXAFS), we can demonstrate that both electronic and local structures of MOFs were almost unchanged between fresh samples and those under the activated/adsorbed/desorbed conditions. This indicates that the CO<sub>2</sub> adsorption of MOFs is mainly governed by the physical driving force. On the other hand, the chemical transformation, *i.e.* elimination of water in MOFs structure by the activation (13.3 kPa, 473 K, 12 h), was found for Cu-BTC only.

Received 23rd March 2016

Accepted 19th June 2016

DOI: 10.1039/c6ra07582g

www.rsc.org/advances

## 1 Introduction

The porous structure of metal–organic frameworks (MOFs) materials has been widely used for various applications such as heterogeneous catalyst,<sup>1</sup> gas separation<sup>2</sup> and drug delivery,<sup>3</sup> because of their larger diversity and flexibility in composition and structure. Carbon dioxide (CO<sub>2</sub>) is a major greenhouse gas that mainly contributes to the global warming causing climate changes, which is now one of the greatest environmental challenges worldwide. Thus, carbon capture and storage (CCS), where carbon dioxide is removed from industrial flue gases have attracted considerable attention.<sup>4,5</sup> The adsorptive progress by MOFs materials is a feasible way for CCS, since most of the MOFs materials have 3D structures incorporating uniform pores and a network of channels possessing extremely large surface area and pore volume.<sup>5</sup>

Recently, a lot of researchers have focused on the structure and chemistry of MOFs for the CCS process, aiming to promote the efficiency CO<sub>2</sub> adsorption and the stability of MOFs during the cyclic adsorption/desorption steps.<sup>6,7</sup> For instance, BASF has commercialized a series of MOFs with different metals and linkers, such as Basolite A100 (MIL-53),<sup>8</sup> C300 (HKUST-1 or Cu-

BTC),<sup>9</sup> F300 (Fe-BTC),<sup>10</sup> Z1200 (ZIF-8),<sup>11</sup> Basosiv M050,<sup>12</sup> *etc.* Among these materials, copper benzene-1,3,5-tricarboxylate (Cu-BTC), first reported by Chui *et al.*<sup>9</sup> was one of the most frequently investigated MOFs for gas adsorption and storage. Iron 1,3,5-benzenetricarboxylate (Fe-BTC) is similarly widely available, with pore size of 22 Å and BET specific surface area of 1500 m<sup>2</sup> g<sup>-1</sup>.<sup>10</sup> Fe-BTC has been successfully used in separation of small organic compounds in liquid phase,<sup>13</sup> exhibiting high catalytic activity for a large variety of reactions requiring Lewis acidity. Additionally, 2-methylimidazole zinc salt (ZIF-8) also presents a high specific surface area (1300–1800 m<sup>2</sup> g<sup>-1</sup>), thermal stability up to 673 K and good chemical stability in water, alkaline solutions and organic solvents.<sup>14</sup>

On the other hand, multiple characterization means such as X-ray diffraction (XRD),<sup>14–17</sup> scanning electron microscope (SEM)<sup>18–20</sup> and X-ray absorption fine structure (XAFS),<sup>17,21,22</sup> have been utilized to understand the so-called “structure–activity” relationship in MOFs. Among them, XAFS is a powerful tool to detect the electronic structure and local chemistry of metals in MOFs. It takes advantages of elementally sensitive, broad detection limits from ppm scale to 100 wt%, good for both crystallized solids and amorphous matters, as well as easy to run *in situ* measurement without damaging the tested samples. Particularly, X-ray absorption near edge spectroscopy (XANES) can provide structural information on oxidation state and charger transfer of metals, and extended X-ray absorption fine structure (EXAFS) can give hints in the short-range local

<sup>a</sup>Department of Chemistry, College of Science, Shanghai University, Shanghai 200444, China

<sup>b</sup>Shanghai Synchrotron Radiation Facility, Shanghai Institute of Applied Physics, Chinese Academy of Sciences, Shanghai 201204, China. E-mail: lilina@sinap.ac.cn

structure, *i.e.* bond distance, coordination number and Debye–Waller (D.W.) factors of first (M–O or M–N) and/or second (M–M) shells for MOFs. For instance, Prestipino *et al.* carried out *ex situ* XAFS measurements on Cu-BTC and determined the corresponding structural evolutions on oxidation state and local coordinated structure of copper atom during different chemical circumstances.<sup>21</sup>

Therefore, in this paper, we tried to carry out the XAFS tests for the MOFs samples at the different steps of fresh, activated, CO<sub>2</sub> adsorption/desorption, to determine the structural evolutions on the three commercial MOFs (Cu-BTC, Fe-BTC and ZIF-8) during the CO<sub>2</sub> adsorption experiments, and to investigate the physical or chemical transformations in MOFs system for CO<sub>2</sub> capture.

## 2 Experimental

### 2.1 Sample

The MOFs of Cu-BTC, Fe-BTC and ZIF-8 were purchased from Sigma Aldrich under trademark Basolite C300, Basolite F300 and Basolite Z1200, respectively. These commercial samples were investigated under the following conditions: (i) “fresh”, directly used without any further purification or modifications; (ii) “activated”, after degassed in vacuum while heated; (iii) “adsorbed”, after room-temperature (298 K) atmosphere-pressure (103 kPa) CO<sub>2</sub> adsorption; (iv) “desorbed”, after the sequential measurements of CO<sub>2</sub> adsorption–desorption.

### 2.2 Characterization

The CO<sub>2</sub> adsorption–desorption measurements were performed on a Micromeritics ASAP 2020 instrument at room temperature (298 K) up to atmosphere pressure (103 kPa). Samples of Cu-BTC, Fe-BTC and ZIF-8 were degassed in vacuum overnight (>12 h) at the temperatures of 473, 423 and 373 K, respectively. The nitrogen adsorption–desorption measurements were performed on an ASAP2020-HD88 analyzer (Micromeritics Co. Ltd.) at 77 K. The BET specific surface areas were calculated from data in the relative pressure range between 0.05 and 0.20. The powder XRD characterization was conducted on a Bruker D8 Advance diffractometer (40 kV, 40 mA) with a scanning rate of 5° min<sup>-1</sup>, using Cu K<sub>α1</sub> radiation ( $\lambda = 1.54056 \text{ \AA}$ ). The corresponding XRD patterns were collected from 5 to 50° with a step of 0.02°. The  $2\theta$  angles were calibrated with a  $\mu\text{m}$ -scale alumina disc. The powder samples after grinding were placed inside a quartz-glass sample holder for each test. With the software “LAPOD” of least-squares refinement of cell parameter “*a*” from powder data by Cohen’s method.<sup>41,42</sup> The SEM experiments were carried out on a Phenom ProX scanning electron microscopy (Sodium Complex Scientific Instrument Co., Ltd) with a working voltage of 10 kV. The transmission electron microscopy (TEM) and high-resolution TEM (HRTEM) measurements were applied on a Philips Tecnai G<sup>2</sup> F20 instrument at 200 kV. All the tested samples were sonicated in ethanol about 10 min, and then a drop of this dispersed suspension was placed on an ultra-thin (3–5 nm in thickness) carbon film-coated Cu grid. The as-

formed sample grid was dried naturally under ambient conditions before inserted into the sample holder.

### 2.3 X-ray absorption fine structure (XAFS)

The XAFS spectra at Fe K-edge (7112 eV), Cu K-edge ( $E_0 = 8979 \text{ eV}$ ) and Zn K-edge ( $E_0 = 9659 \text{ eV}$ ) were performed at BL14W1 beam line of Shanghai Synchrotron Radiation Facility (SSRF) operated at 3.5 GeV under “top-up” mode with a constant current of 240 mA. The activated, adsorbed and desorbed MOFs powders were tightly sealed inside the sample tubes and opened just before the measurements to decrease the possibility of exposure to air. The XAFS data were recorded under transmission mode with high-flux ion chambers. Athena and Artemis codes were used to extract the data and fit the profiles. For the XANES part, the experimental absorption coefficients as function of energies  $\mu(E)$  were processed by background subtraction and normalization procedures, and reported as “normalized absorption”. Based on the normalized XANES profiles, the oxidation state of copper (Cu<sup>2+</sup>/Cu<sup>+</sup>/Cu<sup>0</sup>), iron (Fe<sup>3+</sup>/Fe<sup>2+</sup>/Fe<sup>0</sup>) or zinc (Zn<sup>2+</sup>/Zn<sup>0</sup>) can be determined by comparison with standards. For the EXAFS part, the Fourier transformed (FT) data in *R* space were analyzed by applying 1<sup>st</sup> shell approximation model for the Cu–O, Fe–O or Zn–N shell. The passive electron factors,  $S_0^2$ , were determined by fitting the experimental Cu, Fe or Zn foil data and fixing the Cu–Cu, Fe–Fe or Zn–Zn coordination number (CN) to be 12, 8 + 6 or 6 + 6 and then fixed for further analysis of the measured samples. The parameters describing the electronic properties (*e.g.*, correction to the photoelectron energy origin,  $E_0$ ) and local structure environment including CN, bond distance and D.W. factor around the absorbing atoms were allowed to vary during the fit process. The fitted ranges for *k* were selected to be  $k = 2.5\text{--}11.2$ ,  $2.6\text{--}11.3$  and  $2.4\text{--}12.3 \text{ \AA}^{-1}$  ( $k^3$  weighted) for Fe, Cu and Zn samples. The Fourier transformed (FT) data in *R* space were analyzed by selecting  $R = 1.16\text{--}1.86$  (Cu–O),  $1.00\text{--}1.93$  (Fe–O) and  $1.00\text{--}1.92$  (Zn–N)  $\text{\AA}$  ( $k^3$  weighted), respectively.

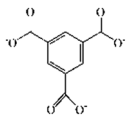
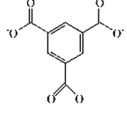
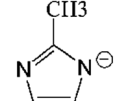
## 3 Results and discussion

### 3.1 CO<sub>2</sub> adsorption and related structural changes

Table 1 shows that Cu-BTC and Fe-BTC have the same organic ligand of 1,3,5-benzenetricarboxylate, while ZIF-8 is based on Zn<sup>2+</sup> atoms linked to nitrogen of imidazolate anions. The BET surface areas for these MOFs samples were determined by the N<sub>2</sub> adsorption measurement as 1522, 1009, 1390 m<sup>2</sup> g<sup>-1</sup> for Cu-BTC, Fe-BTC and ZIF-8, respectively, which is in good agreement with the data from company (Cu-BTC: 1500–2100 m<sup>2</sup> g<sup>-1</sup>; Fe-BTC: 1300–1600 m<sup>2</sup> g<sup>-1</sup>; ZIF-8: 1300–1800 m<sup>2</sup> g<sup>-1</sup>).

In our work, we carried out the CO<sub>2</sub> adsorption/desorption experiments at room temperature (298 K) and ambient pressure (103 kPa). Fig. 1 exhibits that all the measured MOFs (Cu-BTC, Fe-BTC and ZIF-8) have the same H3 type of hysteresis loops associated with the isotherm, indicating their similar CO<sub>2</sub> adsorption behavior in our study. According to the description by IUPAC, this type of hysteresis loop can be attributed to the adsorption of nonpolar gases (CO<sub>2</sub> in this work), which normally

Table 1 Physical properties of MOFs

Sample	Metal	Organic ligand	Surface area <sup>a</sup> (m <sup>2</sup> g <sup>-1</sup> )	CO <sub>2</sub> adsorption <sup>b</sup> (cm <sup>3</sup> g <sup>-1</sup> )	Primary size <sup>c</sup> (μm)	Secondary size <sup>d</sup> (nm)
Cu-BTC	Cu <sup>2+</sup>		1522	73.2	3–10	>1000
Fe-BTC	Fe <sup>3+</sup>		1009	15.9	1–2	20–50
ZIF-8	Zn <sup>2+</sup>		1390	10.4	<1	200–300

<sup>a</sup> Calculated from N<sub>2</sub> adsorption points in the relative pressure range between 0.05 and 0.20. <sup>b</sup> Calculated from CO<sub>2</sub> adsorption/desorption profile at 103 kPa. <sup>c</sup> Determined by SEM. <sup>d</sup> Determined by TEM.

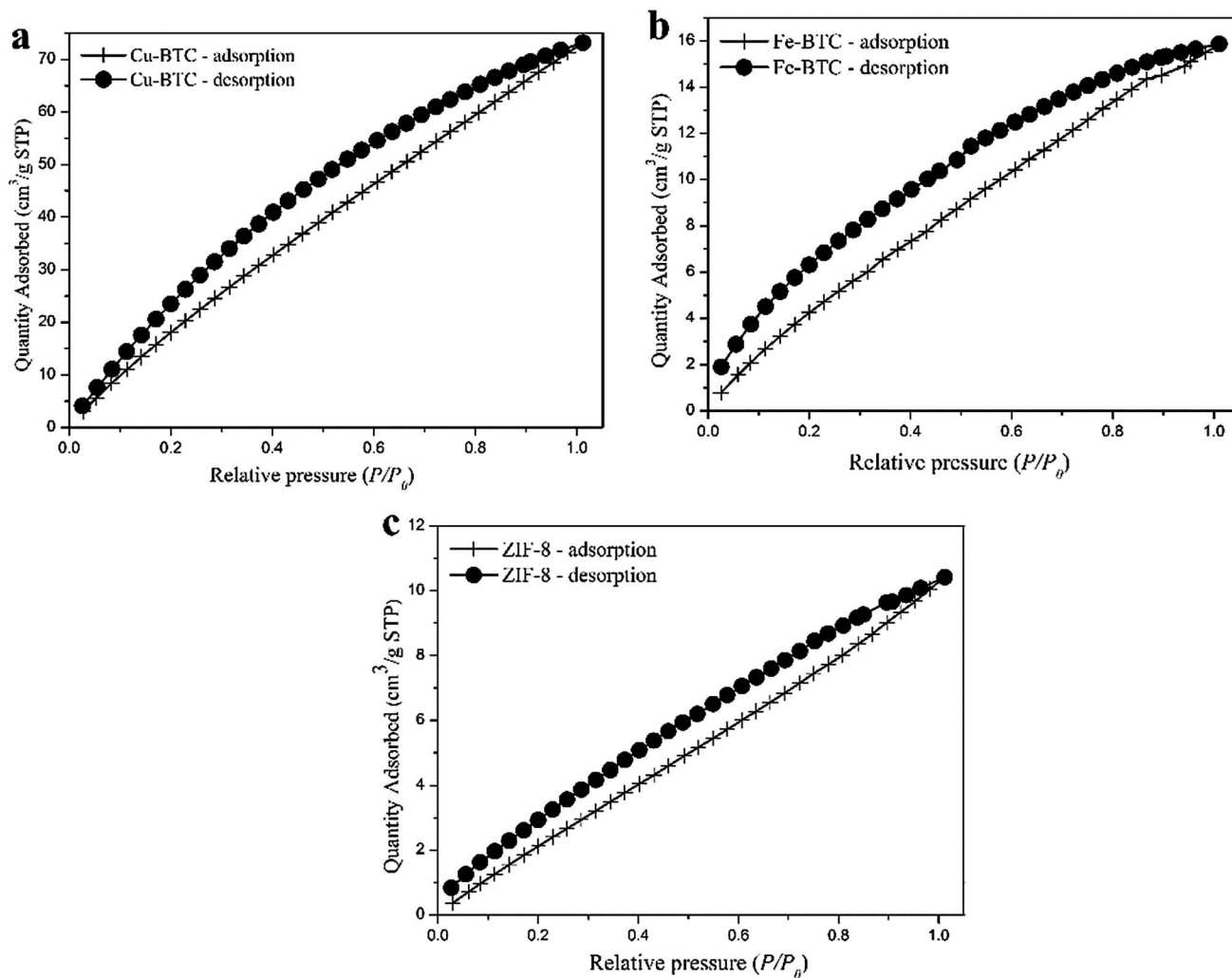


Fig. 1 CO<sub>2</sub> adsorption–desorption isotherms at 298 K ( $P_0 = 101$  kPa) for MOFs: (a) Cu-BTC; (b) Fe-BTC and (c) ZIF-8.

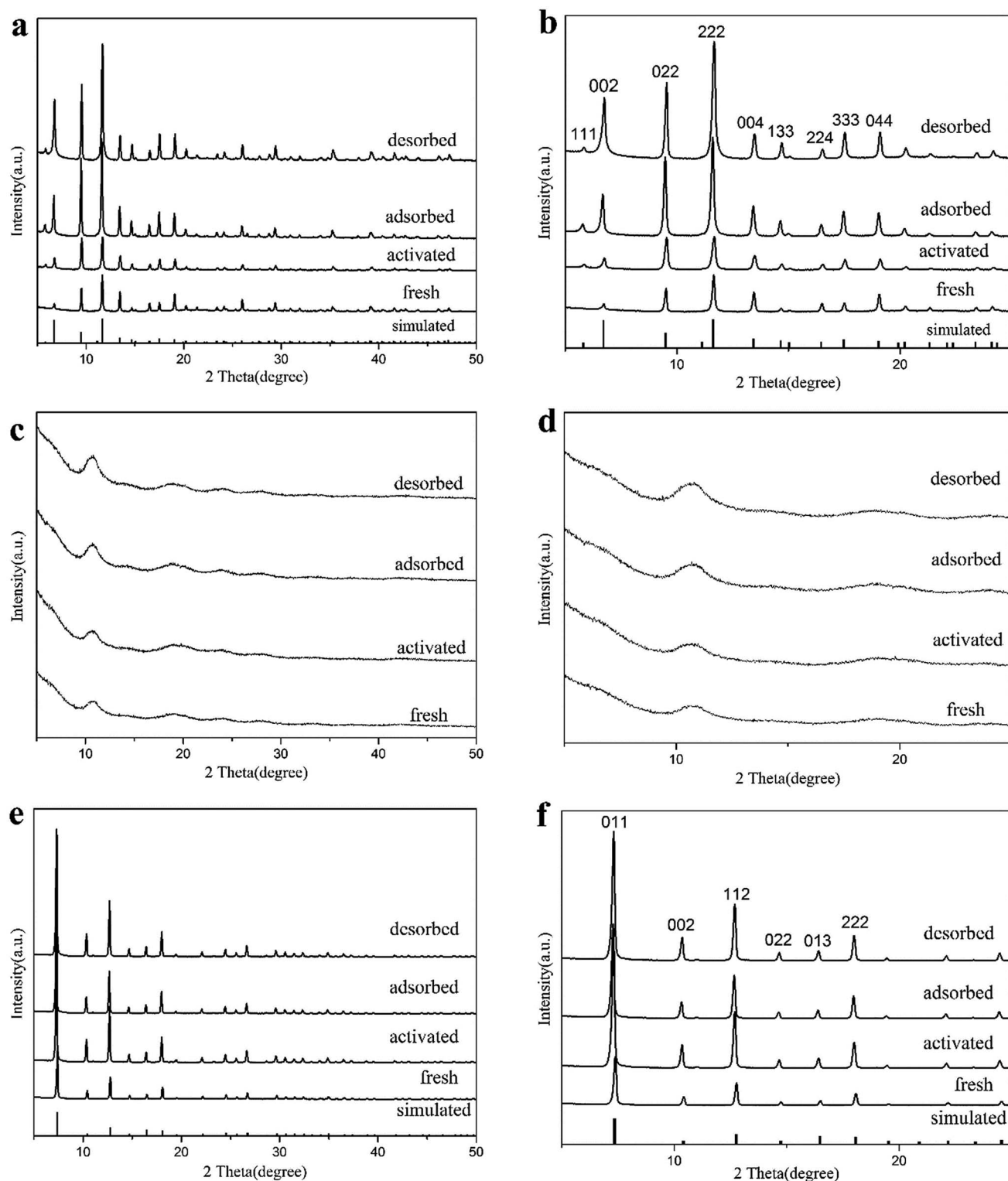


Fig. 2 XRD patterns in full (a, c and e) and enlarged (b, d and f) scales for MOFs: (a and b) Cu-BTC; (c and d) Fe-BTC and (e and f) ZIF-8.

given by microporous materials (*e.g.* montmorillonite clays) or the aggregates of nanocrystals (*e.g.* platy particles).<sup>23</sup> The corresponding calculated CO<sub>2</sub> adsorption amounts are 73.2, 15.9 and 10.4 cm<sup>3</sup> g<sup>-1</sup> for Cu-BTC, Fe-BTC and ZIF-8, respectively.

Till now, over 100 individual MOFs with single-component adsorption of CO<sub>2</sub> have been reported, in which the isotherm measurements were obtained at temperatures from 195 to 353 K with pressures ranging from 6 to 100 kPa or up to 30 MPa.<sup>24</sup> For Cu-BTC and ZIF-8, the largest adsorption amounts reported so

**Table 2** Lattice constants (*a*) of Cu-BTC and ZIF-8 in different conditions

Sample	<i>a</i> (Å)	Sample	<i>a</i> (Å)
Cu-BTC	Simulated <sup>a</sup>	ZIF-8	Simulated
	26.343(5) <sup>b</sup>		16.991(1)
	Fresh		Fresh
	26.3011(3)		16.9706(14)
	Activated		Activated
	26.2427(13)		17.0802(19)
	Adsorbed		Adsorbed
	26.3896(14)		17.1099(27)
	Desorbed		Desorbed
	26.2530(14)		17.0770(16)

<sup>a</sup> From CSD (refcode: FIQCEN) for Cu-BTC and CSD (refcode: VELVOY01) for ZIF-8. <sup>b</sup> The numbers in brackets are experimental errors.

far were 14 mmol g<sup>-1</sup> at 303 K/4 MPa (ref. 25) and 315.5 mg g<sup>-1</sup> at 298 K/5 MPa.<sup>26</sup> Comparable to our testing conditions, the adsorption amount at room temperature and ambient atmosphere measured by previous groups were 65–115 (ref. 27–31) and 9–16 cm<sup>3</sup> g<sup>-1</sup> (ref. 32–34) for Cu-BTC and ZIF-8, respectively. Here, our current experimental data in Table 1 are well consistent with these reports. Although Fe-BTC has not widely been investigated for CO<sub>2</sub> capture, its adsorption amount was nearly equal to that of ZIF-8 in our work (see Table 1). Therefore, the results of CO<sub>2</sub> adsorption/desorption experiments confirmed that the selected three commercial MOFs samples are appropriate to the CCS studies in the following sections.

The crystal structure of three commercial MOFs samples during different steps (fresh, activated, adsorbed and desorbed) were determined by XRD. Fig. 2a and b display that the well-resolved pattern of fresh Cu-BTC, which is in good agreement with the XRD data reported by Dhakshinamoorthy *et al.*<sup>15</sup> and Lin *et al.*<sup>16</sup> After the following CO<sub>2</sub> adsorption/desorption processes, the diffraction patterns or peak-positions of activated/adsorbed/desorbed MOFs were kept the same as the fresh sample, revealing that no phase transfer happened during the CO<sub>2</sub> adsorption/desorption at room temperature and ambient pressure. In contrast to Cu-BTC, the XRD pattern of fresh Fe-BTC in Fig. 2c and d show weak and wide diffraction peaks, indicating its low crystallinity or amorphous nature. This is consistent to the previous findings by Sciortino *et al.*<sup>17</sup> The pattern of ZIF-8 (see Fig. 2e and f) also confirms the main features associated with the ZIF-8 phase reported previously.<sup>14</sup> Again, for Fe-BTC and ZIF-8, there was no observed changes in crystal phase between fresh, activated, adsorbed and desorbed MOFs.

Additionally, we calculated the lattice constants (*a*) of Cu-BTC and ZIF-8 in fresh/activated/adsorbed/desorbed conditions *via* least square method by using the LAPOD software. It can be seen from Table 2 and Fig. 3 that the *a* values of the investigated MOFs samples were slightly changed after each step, but close to those from crystallographic database. Previously, Prestipino *et al.* observed that the removal of water molecule from the Cu-BTC reduced its cell volume.<sup>21</sup> In our work, the *a* value of Cu-BTC also decreased from fresh (26.3011 Å) to activated (26.2427 Å). Meanwhile, the following procedures of adsorbed (26.3896 Å) and desorbed (26.2530 Å) showed inconsistent impacts on lattice constants, revealing the complicated transformations in CO<sub>2</sub> adsorption/desorption process for Cu-BTC. As for ZIF-8 (Fig. 3b), the corresponding cell dimensions displayed a monotone increasing from fresh (16.9706 Å) to activated (17.0802 Å), and to adsorbed (17.1099 Å), plus a slight decreasing on desorbed (17.0770 Å), which indicates the probably different mechanisms between Cu-BTC and ZIF-8.

The morphologies of the different MOFs samples at the μm scale were identified by SEM. Cu-BTC displays the aggregates of big (3–10 μm) regular crystals with well-define polygonal surfaces (Fig. 4a); while for Fe-BTC, smaller irregular crystals with the size of mostly less than 2 μm were determined (Fig. 4b); as for ZIF-8, more small-size (<1 μm) particles were observed in SEM (Fig. 4c). However, for all the three MOFs materials, their morphologies were maintained after the activation/adsorption/desorption process. It gives a hint that the MOFs crystals were highly stable during the CO<sub>2</sub> adsorption/desorption experiments.

Since SEM only provided the exterior morphologies, including the shape and size of secondary (aggregated) particles, we further to investigate the shape and size of primary (single) crystals of MOFs by the aids of TEM. In microdomain, the Cu-BTC particles are well-defined and big (Fig. 5a1), which almost impenetrable to the electron beam so as to no further information obtained in HRTEM (Fig. 5a2); the Fe-BTC crystals are small-size spheres between 20 and 50 nm (Fig. 5b1), and no clear lattice fringes can be identified in HRTEM (Fig. 5b2), which is in good agreement with the XRD results on the amorphous Fe-BTC; the morphology of ZIF-8 is similar to that of Cu-BTC, but with smaller crystal size around 200–300 nm (Fig. 5c1), while partially impenetrable to the electron beam (Fig. 5c2). These TEM results were very close to the previous reports.<sup>33,35–37</sup>

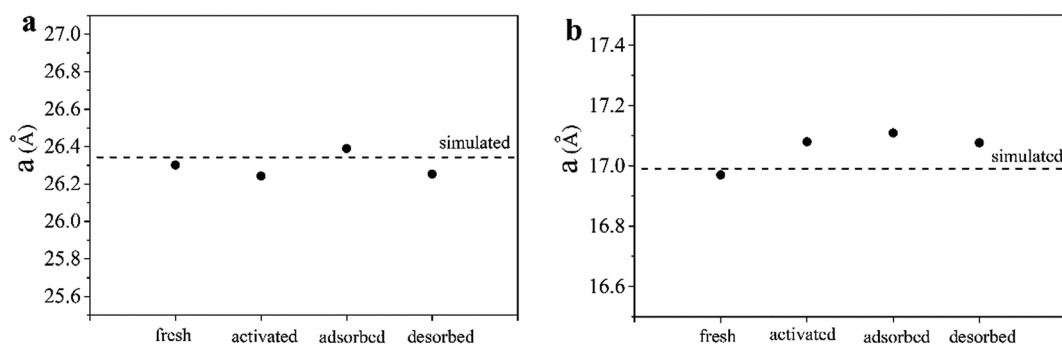


**Fig. 3** Lattice constants of (a) Cu-BTC and (b) ZIF-8 in different conditions.

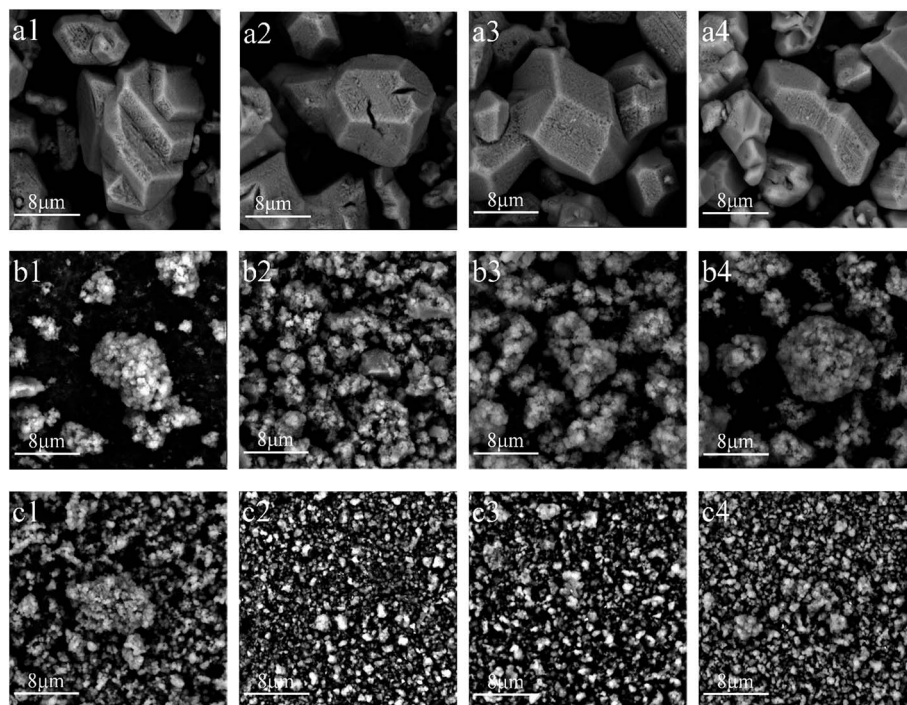


Fig. 4 SEM images of MOFs for (a) Cu-BTC, (b) Fe-BTC and (c) ZIF-8 of (1) fresh, (2) activated, (3) adsorbed and (4) desorbed.

### 3.2 Short-range structure determined by XAFS

As discussed as above, the conventional characterizations including XRD, SEM and TEM cannot provide the reliable information on specific structure around the measured metal (Cu, Fe, Zn) atoms, which are very important to demonstrate the CO<sub>2</sub> adsorption mechanism. Here, XAFS technique was used to investigate the structure in the three MOFs samples, which is elemental sensitive and very powerful to determine the electronic and local structure of metals. Besides, the XAFS measurement can be performed under harsh circumstances

such as high temperature (up to more than 1273 K), high pressure (up to GPa) and various gaseous atmospheres (air, CO<sub>2</sub>, H<sub>2</sub>, *etc.*).

The Cu K-edge XANES spectrum of CuO reference (Fig. 6a) shows a pre-edge peak around 8985 eV, attributed to the dipole-allowed  $1s \rightarrow 4p$  electron transition for Cu(II), plus a very weak peak around 8978 eV (see marks in Fig. 6a), ascribed to the quadrupolar transition of  $1s \rightarrow 3d$ .<sup>22</sup> In order to be observed more visually, we converted the XANES profile to the derivative pattern. Fig. 6b exhibits that for fresh Cu-BTC, the dipole-

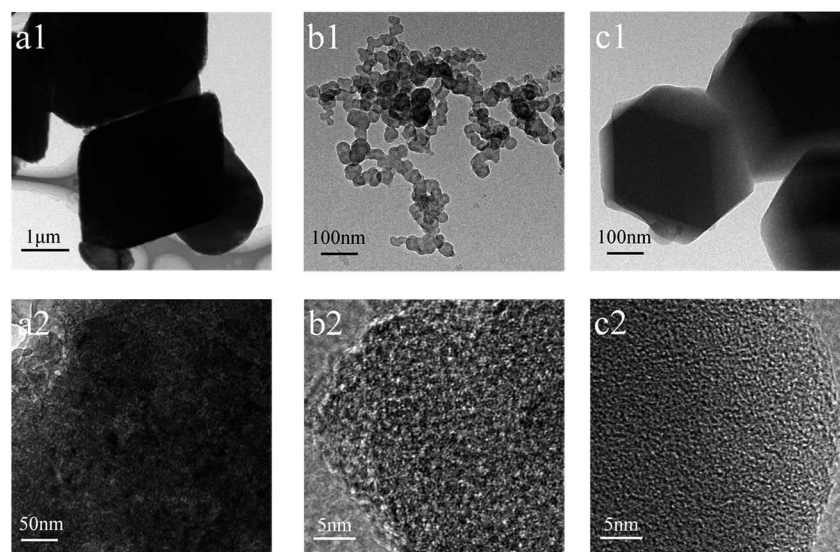


Fig. 5 TEM (1) and HRTEM (2) images of fresh MOFs samples: (a) Cu-BTC; (b) Fe-BTC; (c) ZIF-8.

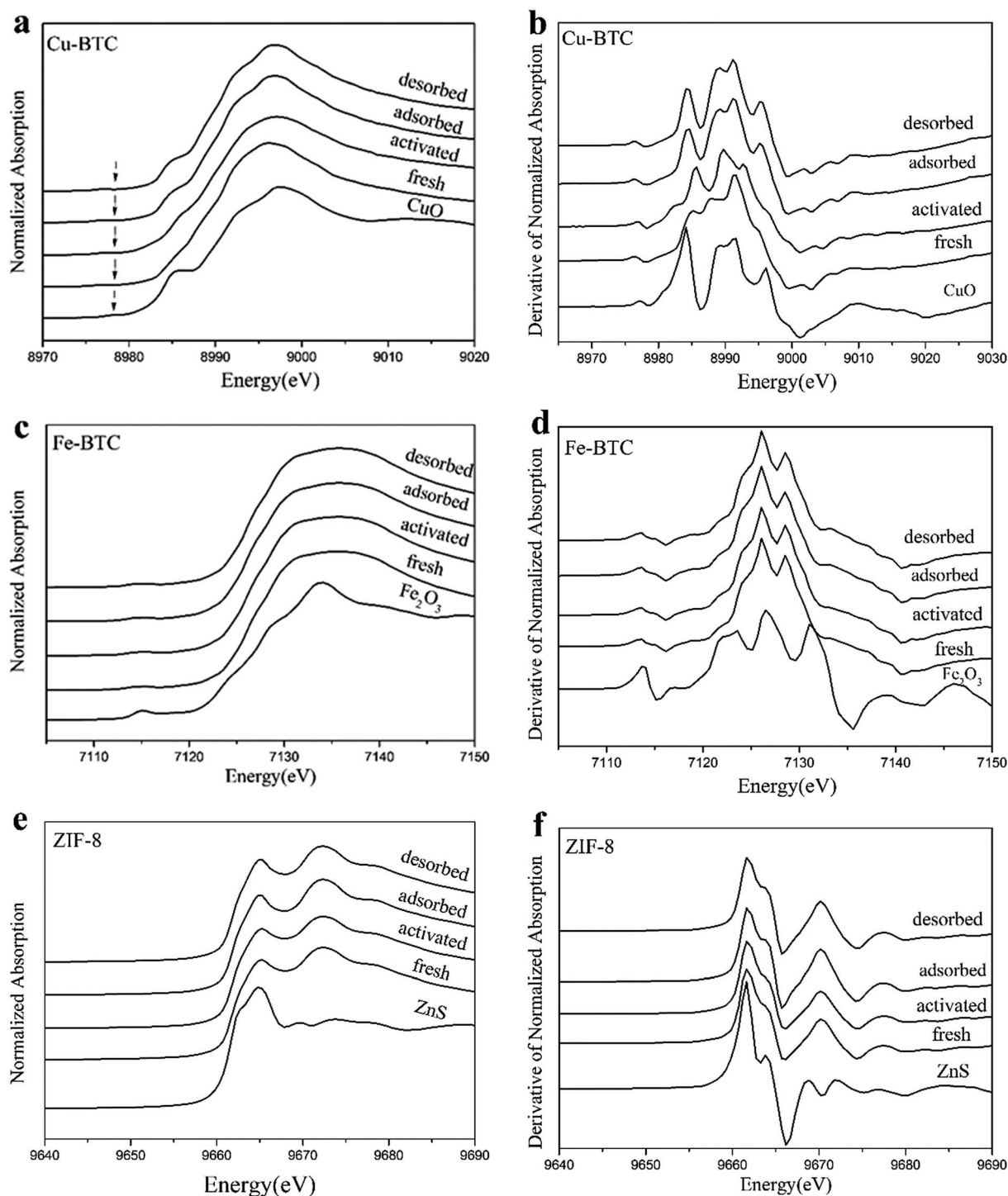


Fig. 6 XANES profiles of the MOFs samples: (a and b) Cu-BTC; (c and d) Fe-BTC; (e and f) ZIF-8.

allowed electron transition around 8985 eV is not pronounced, possibly due to the hydration effect.<sup>21</sup> As for the activated, adsorbed and desorbed spectra, the  $\text{Cu}^{2+}$  features were maintained in XANES (Fig. 6a). However, the peak intensity of quadrupolar transition around 8978 eV is significantly enhanced (Fig. 6b), if compared to the fresh sample, indicating the dehydrating process happened during the activation (out-gassing) step.

The Fe K-edge XANES spectrum of  $\text{Fe}_2\text{O}_3$  reference (Fig. 6c) shows a pre-edge peak around 7115 eV, which can be assigned to the  $1s \rightarrow 3d$  electron transition of iron component.<sup>17</sup> The profile of fresh Fe-BTC is similar to that of the  $\text{Fe}^{3+}$  ( $\text{Fe}_2\text{O}_3$ ) standard, and remained unchanged after the sequential processes of activated, adsorbed and desorbed (Fig. 6c). The derivative pattern of Fe-BTC is less sharper and has slight shift of peak-position in the range of 7120–7135 eV, if compared to

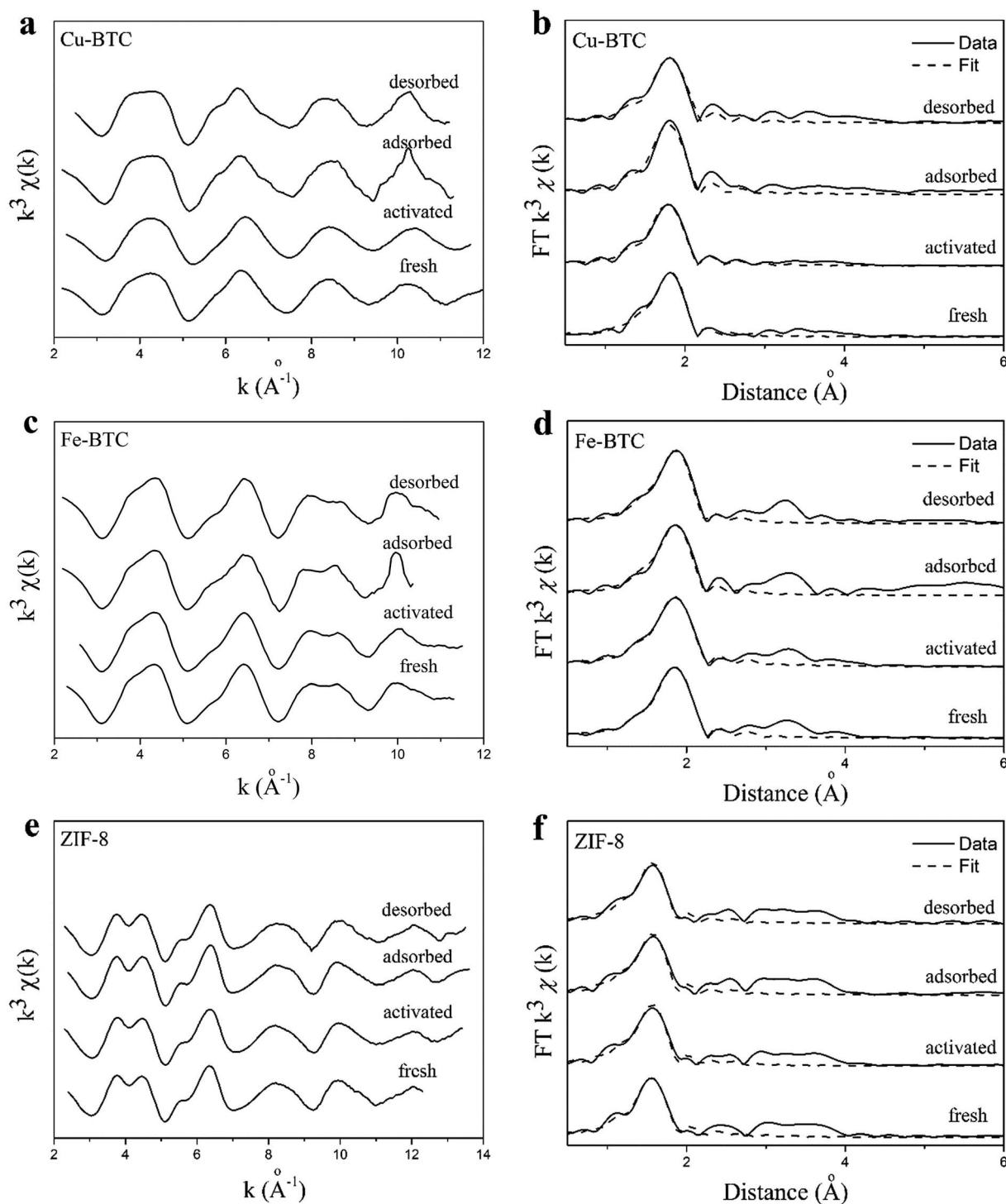


Fig. 7 EXAFS profiles in  $k$  (a, c and e) and  $R$  space with the fitted curves (b, d and f) of MOFs: (a and b) Cu-BTC; (c and d) Fe-BTC; (e and f) ZIF-8.

that of  $\text{Fe}_2\text{O}_3$ , revealing the different coordination environment for Fe-BTC 1.952. Different from Cu-BTC, the activated, adsorbed and desorbed Fe-BTC samples were almost identical to the fresh materials in both the XANES profiles (Fig. 6c) and the derivative pattern (Fig. 6d). Previously, it has been reported that Fe-BTC is very stable and not susceptible to dramatic changes when the atmosphere is modified from air to vacuum or when adsorbed water molecules are removed by activation.<sup>17</sup>

The Zn K-edge XANES spectrum is much complicated, and the corresponding profiles can be affected by oxidation state or crystal symmetry of zinc, as well as the surrounding ligands or metal-support interaction. The edge position in XANES of fresh ZIF-8 is partially close to that of ZnS reference (Fig. 6e), but the post-edge profile is distinctly different in the multiple scattering range of 9665–9685 eV. As for the derivative curve of ZIF-8 (Fig. 6f), the characteristic (edge) peak at 9662 eV is constant



**Table 3** EXAFS fitting results ( $R$ : distance; CN: coordination number; D.W.: Debye–Waller factor;  $\Delta E_0$ : inner potential correction to account for the difference in the inner potential between the sample and the reference) of MOFs under different conditions

Sample		M–O or M–N		$\Delta E_0$ (eV)	D.W.
		$R$ (Å)	CN		
Cu-BTC	Fresh	1.95 ± 0.01	3.9 ± 0.2	−0.1 ± 0.5	0.0054 ± 0.0005
	Activated	1.93 ± 0.01	3.8 ± 0.2		
	Adsorbed	1.95 ± 0.01	4.5 ± 0.3		
	Desorbed	1.96 ± 0.01	4.3 ± 0.2		
Fe-BTC	Fresh	2.00 ± 0.01	5.9 ± 0.1	1.3 ± 0.2	0.0075 ± 0.0003
	Activated	2.00 ± 0.01	5.9 ± 0.1		
	Adsorbed	2.00 ± 0.01	5.7 ± 0.3		
	Desorbed	2.00 ± 0.01	6.0 ± 0.3		
ZIF-8	Fresh	1.99 ± 0.01	4.5 ± 0.3	4.0 ± 0.5	0.0046 ± 0.0004
	Activated	1.99 ± 0.01	4.5 ± 0.3		
	Adsorbed	1.99 ± 0.01	4.4 ± 0.3		
	Desorbed	1.99 ± 0.01	4.4 ± 0.3		

for the fresh, activated, adsorbed and desorbed samples, confirming that the  $\text{Zn}^{2+}$  species in ZIF-8 was not reduced to  $\text{Zn}^0$  in the  $\text{CO}_2$  adsorption/desorption processes.

The  $k^3$ -weighted EXAFS spectra in  $k$  and  $R$  spaces are included in Fig. 7. The profiles for each MOFs between fresh, activated, adsorbed and desorbed samples are very close, without significant changes. Thus, the short-range local structures around metals (Cu, Fe, Zn) are similar under different conditions. Furthermore, we carried out the EXAFS fittings on the  $R$  space to determine the structural parameters such as distance ( $R$ ), coordination number (CN), Debye–Waller (D.W.) factor and inner potential correction to account for the difference in the inner potential between the sample and the reference ( $\Delta E_0$ ). Since the oxidation state of metals are identical and the coordinated atoms are the same within each MOFs for fresh, activated, adsorbed and desorbed samples, we applied group fit on D.W. and  $\Delta E_0$  to decrease the total parameters to be decided by EXAFS simulation. The fitted curves (dot line) are displayed in Fig. 7b, d and f and the corresponding calculated values are listed in Table 3.

For Cu-BTC, the copper atom is coordinated with oxygen from organic ligand. Table 3 exhibits that CN of Cu–O is 3.9 and the distance is 1.95 Å in the fresh sample, which are well consistent with the theoretic numbers (CN = 4,  $R$  = 1.952 Å) according to the single-crystal MOFs structure.<sup>9</sup> Upon activation, CN was kept the same (3.8) while the distance of Cu–O decreased to 1.93 Å (Table 3). This slight shorter distance of Cu–O could be caused by the loss of coordinated water molecules as reported by Prestipino,<sup>21</sup> the coordination between copper atoms and ligand oxygen with stronger interaction replaces the eliminated Cu– $\text{H}_2\text{O}$  chemical bonding. However, we found that the CN values of Cu–O for Cu-BTC after  $\text{CO}_2$  adsorption and desorption were significantly enhanced to 4.5 and 4.3, respectively, while the corresponding distances recovered to 1.95–1.96 Å (see Table 3, Fig. 8a and b). These results demonstrate that (1)  $\text{CO}_2$  adsorption in Cu-BTC may be related to the chemical bonding between copper center and oxygen from  $\text{CO}_2$ , which is an extra contribution besides the major Cu–O in fresh MOFs; (2) this chemical bonding may not disappear completely after the

desorption step in the  $\text{CO}_2$  adsorption experiment. Although XAFS is macroscopic characterization which averages all the contributions around centered metals, the changes in coordination number and distance can also give hints on the mechanism for  $\text{CO}_2$  capture in MOFs.

As for Fe-BTC, Table 3 shows that the CN and  $R$  values in fresh sample are 5.9 and 2.00 Å, respectively, which is in good agreement with the previous report (CN = 5.2,  $R$  = 2.00 Å).<sup>17</sup> Fig. 8c and d display that these structural parameters were maintained constantly after the sequential processes of activation, adsorption and desorption, if considering the fitting errors. From these results, we can exclude the presence of adsorbed water in fresh Fe-BTC and the formation of chemical bonding between iron and  $\text{CO}_2$  molecule during the adsorption step. Similar to Fe-BTC, the CN and  $R$  values of Zn–N in ZIF-8 are totally identical in spite of different treatment conditions (fresh, activated, adsorbed and desorbed, see Table 3, Fig. 8e and f). It indicates that there was no changes in short-range local structure for zinc atoms in ZIF-8 during the  $\text{CO}_2$  adsorption experiment.

### 3.3 Adsorption mechanism

For the adsorption mechanism on  $\text{CO}_2$  capture by MOFs, previous work emphasized the importance of open metal sites, which are typically obtained by incorporating solvent molecules (*e.g.*  $\text{H}_2\text{O}$ ) as terminal ligands.<sup>38</sup> For instance, MOFs with exposed metal ion sites were performed predominantly on Cu-BTC, and the solvent molecules coordinated at the axial positions of the  $\text{Cu}_2(\text{COO})_4$  paddle-wheel units can be removed to afford open  $\text{Cu}^{2+}$  sites.<sup>9,39</sup> Furthermore, careful handling of the activated samples is essential, since the exposed metal sites probably become hydrated, even with a short-time exposure to ambient moisture.<sup>40</sup> However, as we know that  $\text{CO}_2$  is a typical nonpolar molecule and should physically adsorbed into the porous materials.<sup>38</sup>

To clarify the arguments on  $\text{CO}_2$  adsorption mechanism by MOFs, in this work, we carried out multiple characterization approaches for the three commercially available MOFs samples under different conditions of fresh, activated, adsorbed and

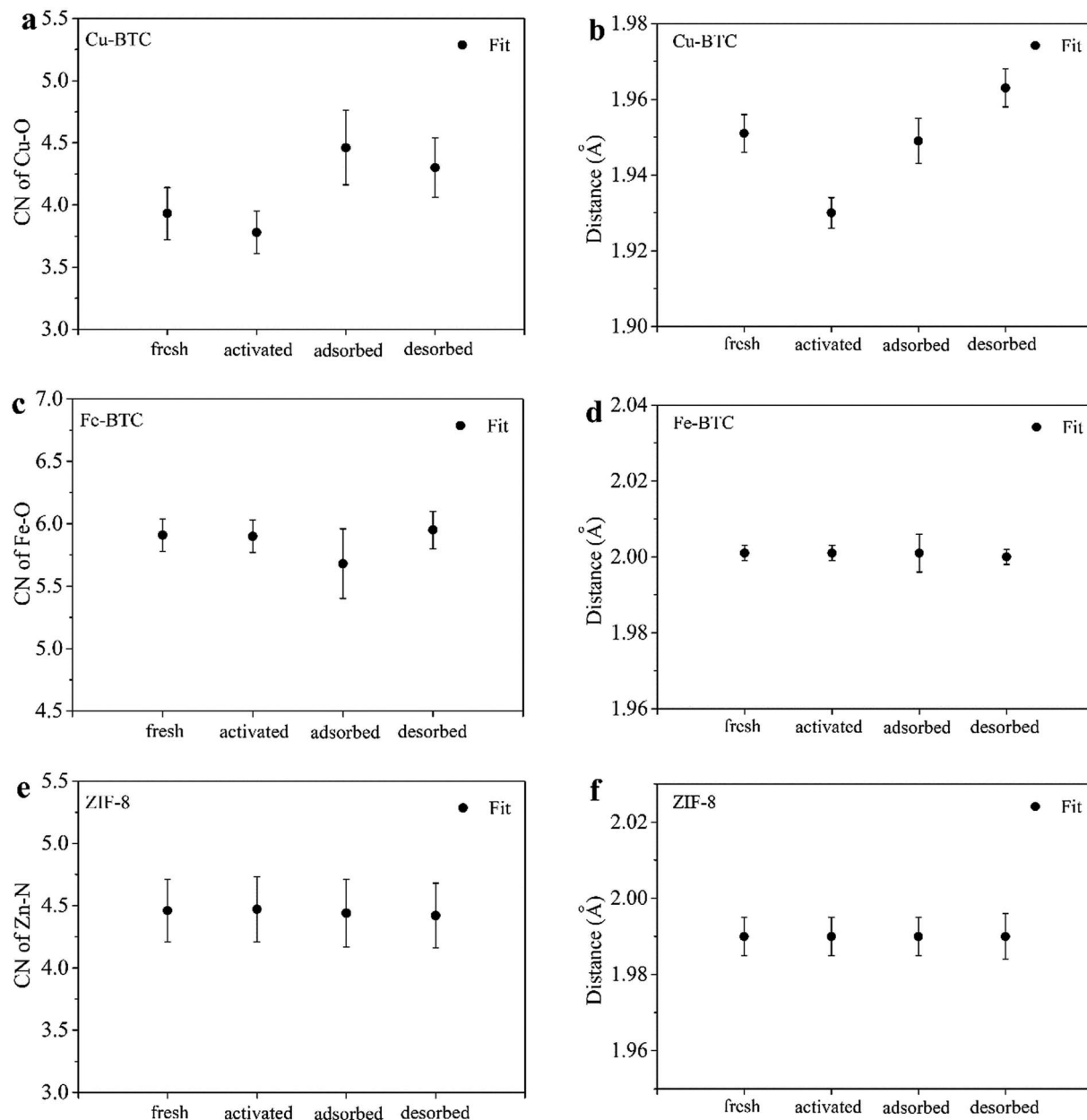


Fig. 8 Coordination numbers (a, c and e), and distances (b, d and f) of MOFs under the different conditions: (a and b) Cu-BTC; (c and d) Fe-BTC; (e and f) ZIF-8.

desorbed. The selected Cu-BTC, Fe-BTC and ZIF-8 show similar CO<sub>2</sub> adsorption amount at room temperature and ambient pressure as the reported values in literature. As discussed as above, the conventional methods including XRD, SEM and TEM show no observable differences on the various testing steps in each MOFs. So, the overall structure of these samples was very stable during the CO<sub>2</sub> adsorption experiments.

Particularly, XAFS technique, including XANES for analysis of oxidation state and EXAFS for refinement of short-range (up to 6–8 Å) local structure, is very powerful to detect the structural evolution around the investigated metal atoms. It can be seen from Fig. 6 (XANES) and Fig. 7 (EXAFS) that the oxidation state and the coordinated structure (distance and coordination

number of first shell) of these three MOFs were almost identical during the different CO<sub>2</sub> adsorption/desorption processes. This clearly discovers that the physical transformation is the main driving force on the CO<sub>2</sub> capture by the pore structure of Cu-BTC, Fe-BTC and ZIF-8, which was consistent with the previous findings, *i.e.* CO<sub>2</sub> adsorbed by porous materials is much more energy efficient than capture by chemical absorbents because physical adsorption requires less energy for regeneration.<sup>6</sup>

On the other hand, we also observed a minor change in XANES spectra between fresh and activated Cu-BTC (Fig. 6a and b), as well as the differences on the fitted coordination number and distance for Cu–O shell between different steps (Table 3,

Fig. 8a and b). This evolution is related to the removal of water in the lattice of Cu-BTC,<sup>21</sup> and the adsorption of CO<sub>2</sub> molecule to form chemical bonding with Cu<sup>2+</sup> center *via* probably Cu–O bond, in which the unsaturated metal ions serve as charge-dense binding sites. All these chemical transformation is unique for Cu-BTC only. From Fig. 1, the hysteresis loops of the three MOFs samples are similar, while Cu-BTC showed 5–7 times higher absorption amount of CO<sub>2</sub> compared to Fe-BTC and ZIF-8, although their BET surface areas (physical adsorption) are similar. Furthermore, we also found that zero CO<sub>2</sub> adsorption amount for the Cu-BTC sample without the elimination of such structural water. Therefore, the chemical transformation, *i.e.* removal of structural water, is also important for the CO<sub>2</sub> capture by MOFs in Cu-BTC.

## 4 Conclusions

In this paper, we investigated the CO<sub>2</sub> adsorption mechanism on three commercial MOFs (Cu-BTC, Fe-BTC and ZIF-8) by multiple characterization approaches. The XRD, SEM and TEM results reveal that the bulk structure of MOFs was very stable during the different conditions (fresh, activated, adsorbed and desorbed) of experiment. However, by the aids of XAFS technique, including XANES analyses and EXAFS fittings, we found that the chemical transformation of dehydration, as well as the interaction between copper and CO<sub>2</sub> molecule, happened for Cu-BTC only; while solely physical driving force was detected for Fe-BTC and ZIF-8 during the CO<sub>2</sub> adsorption measurements.

## Acknowledgements

This work was supported by the youth project of National Natural Science Fund (11405256), Shanghai Municipal Natural Science Foundation (13ZR1447800), and the project of the National Natural Science Foundation of China (U1532120, 21171115).

## References

- 1 A. Dhakshinamoorthy, M. Alvaro and H. Garcia, Metal-organic frameworks as heterogeneous catalysts for oxidation reactions, *Catal. Sci. Technol.*, 2011, **1**, 856–867.
- 2 Q. M. Wang, D. M. Shen, M. Bülow, M. L. Lau, S. G. Deng, F. R. Fitch, N. O. Lemcoff and J. Semancin, Metallo-organic molecular sieve for gas separation and purification, *Microporous Mesoporous Mater.*, 2002, **55**, 217–230.
- 3 C. Y. Sun, C. Qin, X. L. Wang, G. S. Yang, K. Z. Shao, Y. Q. Lan, Z. M. Su, P. Huang, C. G. Wang and E. B. Wang, Zeolitic imidazolate framework-8 as efficient pH-sensitive drug delivery vehicle, *Dalton Trans.*, 2012, **41**, 6906–6909.
- 4 E. S. Kikkinides, R. T. Yang and S. H. Cho, Concentration and recovery of CO<sub>2</sub> from flue gas by pressure swing adsorption, *Ind. Eng. Chem. Res.*, 1993, **32**, 2714–2720.
- 5 A. R. Millward and O. M. Yaghi, Metal-organic frameworks with exceptionally high capacity for storage of carbon dioxide at room temperature, *J. Am. Chem. Soc.*, 2005, **127**, 17998–17999.
- 6 S. Noro, Y. Hijikata, M. Inukai, T. Fukushima, S. Horike, M. Higuchi, S. Kitagawa, T. Akutagawa and T. Nakamura, Highly selective CO<sub>2</sub> adsorption accompanied with low-energy regeneration in a two-dimensional Cu(II) porous coordination polymer with inorganic fluorinated PF<sub>6</sub><sup>−</sup> anions, *Inorg. Chem.*, 2013, **52**, 280–285.
- 7 Y. Liu, J. Liu and Y. S. Lin, Strong binding site molarity of MOFs and its effect on CO<sub>2</sub> adsorption, *Microporous Mesoporous Mater.*, 2015, **214**, 242–245.
- 8 C. Serre, F. Millange, C. Thouvenot, M. Nogues, G. Marsolier, D. Louer and G. Férey, Very large breathing effect in the first nanoporous chromium(III)-based solids: MIL-53 or Cr<sup>III</sup>(OH)·{O<sub>2</sub>C–C<sub>6</sub>H<sub>4</sub>–CO<sub>2</sub>}·{HO<sub>2</sub>C–C<sub>6</sub>H<sub>4</sub>–CO<sub>2</sub>H}<sub>x</sub>·H<sub>2</sub>O<sub>y</sub>, *J. Am. Chem. Soc.*, 2002, **124**, 13519–13526.
- 9 S. S. Y. Chui, S. M. F. Lo, J. P. H. Charmant, A. G. Orpen and I. D. Williams, A chemically functionalizable nanoporous material [Cu<sub>3</sub>(TMA)<sub>2</sub>(H<sub>2</sub>O)<sub>3</sub>]<sub>n</sub>, *Science*, 1999, **283**, 1148–1150.
- 10 K. F. Babu, M. A. Kulandainathan, I. Katsounaros, L. Rassaei, A. D. Burrows, P. R. Raithby and F. Marken, Electrocatalytic activity of Basolite™ F300 metal-organic-framework structures, *Electrochem. Commun.*, 2010, **12**, 632–635.
- 11 R. Banerjee, A. Phan, B. Wang, C. Knobler, H. Furukawa, M. O’Keeffe and O. M. Yaghi, High-throughput synthesis of zeolitic imidazolate frameworks and application to CO<sub>2</sub> capture, *Science*, 2008, **319**, 939–943.
- 12 K. Schuchmann and V. Müller, Direct and reversible hydrogenation of CO<sub>2</sub> to formate by a bacterial carbon dioxide reductase, *Science*, 2013, **342**, 1382–1385.
- 13 A. Centrone, E. E. Santiso and T. A. Hatton, Separation of chemical reaction intermediates by metal-organic frameworks, *Small*, 2011, **17**, 2356–2364.
- 14 K. S. Park, Z. Ni, A. P. Cote, J. Y. Choi, R. Huang, F. J. Uribe-Romo, H. K. Chae, M. O’Keeffe and O. M. Yaghi, Exceptional chemical and thermal stability of zeolitic imidazolate frameworks, *Proc. Natl. Acad. Sci. U. S. A.*, 2006, **103**, 10186–10191.
- 15 A. Dhakshinamoorthy, M. Alvaro and H. Garcia, Metal-organic frameworks as heterogeneous catalysts for the selective *N*-methylation of aromatic primary amines with dimethyl carbonate, *Appl. Catal., A*, 2010, **378**, 19–25.
- 16 K. S. Lin, A. K. Adhikari, C. N. Ku, C. L. Chiang and H. Kuo, Synthesis and characterization of porous HKUST-1 metal-organic frameworks for hydrogen storage, *Int. J. Hydrogen Energy*, 2012, **37**, 13865–13871.
- 17 L. Sciortino, A. Alessi, F. Messina, G. Buscarino and F. M. Gelardi, Structure of the FeBTC metal-organic framework: a model based on the local environment study, *J. Phys. Chem. C*, 2015, **119**, 7826–7830.
- 18 M. Opanasenko, M. Shamzhy and J. Cejka, Solid acid catalysts for coumarin synthesis by the Pechmann reaction: MOFs *versus* zeolites, *ChemCatChem*, 2013, **5**, 1024–1031.
- 19 R. L. Papporello, E. E. Miro and J. M. Zamaro, Secondary growth of ZIF-8 films onto copper-based foils. Insight into

- surface interactions, *Microporous Mesoporous Mater.*, 2015, **211**, 64–72.
- 20 K. Díaz, M. López-González, L. F. del Castillo and E. Riande, Effect of zeolitic imidazolate frameworks on the gas transport performance of ZIF8-poly(1,4-phenylene ether-ether-sulfone) hybrid membranes, *J. Membr. Sci.*, 2011, **383**, 206–213.
- 21 C. Prestipino, L. Regli, J. G. Vitillo, F. Bonino, A. Damin, C. Lamberti, A. Zecchina, P. L. Solari, K. O. Kongshaug and S. Bordiga, Local structure of framework Cu(II) in HKUST-1 metallorganic framework: spectroscopic characterization upon activation and interaction with adsorbates, *Chem. Mater.*, 2006, **18**, 1337–1346.
- 22 C. Lamberti, S. Bordiga, F. Bonino, C. Prestipino, G. Berlier, L. Capello, F. D'Acapito, F. X. Llabrés i Xamenaab and A. Zecchina, Determination of the oxidation and coordination state of copper on different Cu-based catalysts by XANES spectroscopy *in situ* or in operando conditions, *Phys. Chem. Chem. Phys.*, 2003, **5**, 4502–4509.
- 23 K. S. W. Sing and R. T. Williams, Physisorption hysteresis loops and the characterization of nanoporous materials, *Adsorpt. Sci. Technol.*, 2004, **22**, 773–782.
- 24 J. R. Li, Y. G. Ma, M. Colin McCarthy, J. Sculley, J. Yu, H. K. Jeong, P. B. Balbuena and H. C. Zhou, Carbon dioxide capture-related gas adsorption and separation in metal-organic frameworks, *Coord. Chem. Rev.*, 2011, **255**, 1791–1823.
- 25 L. Hamon, E. Jolimaitre and G. D. Pirngruber, CO<sub>2</sub> and CH<sub>4</sub> separation by adsorption using Cu-BTC metal-organic framework, *Ind. Eng. Chem. Res.*, 2010, **49**, 7497–7503.
- 26 J. Q. Zhu, L. Jiang, C. N. Dai, N. Yang and Z. G. Lei, Gas adsorption in shaped zeolitic imidazolate framework-8, *Chin. J. Chem. Eng.*, 2015, **23**, 1275–1282.
- 27 J. K. Xie, N. Q. Yan, Z. Qu and S. J. Yang, Synthesis, characterization and experimental investigation of Cu-BTC as CO<sub>2</sub> adsorbent from flue gas, *J. Environ. Sci.*, 2012, **24**, 640–644.
- 28 J. Kim, S. H. Kim, S. T. Yang and W. S. Ahn, Bench-scale preparation of Cu<sub>3</sub>(BTC)<sub>2</sub> by ethanol reflux: synthesis optimization and adsorption/catalytic applications, *Microporous Mesoporous Mater.*, 2012, **161**, 48–55.
- 29 H. Wang, Z. G. Qu, W. Zhang, Q. N. Yu and Y. L. He, Experimental and numerical study of CO<sub>2</sub> adsorption on copper benzene-1,3,5-tricarboxylate (Cu-BTC) metal-organic framework, *Int. J. Heat Mass Transfer*, 2016, **92**, 859–863.
- 30 A. O. Yazaydin, A. I. Benin, S. A. Faheem, P. Jakubczak, J. J. Low, R. R. Willis and R. Q. Snurr, Enhanced CO<sub>2</sub> adsorption in metal-organic frameworks *via* occupation of open-metal sites by coordinated water molecules, *Chem. Mater.*, 2009, **21**, 1425–1430.
- 31 F. J. Song, Q. Zhong and Y. X. Zhao, A protophilic solvent-assisted solvothermal approach to Cu-BTC for enhanced CO<sub>2</sub> capture, *Appl. Organomet. Chem.*, 2015, **29**, 612–617.
- 32 S. Xian, F. Xu, C. Ma, Y. Wu, Q. B. Xia, H. Wang and Z. Li, Vapor-enhanced CO<sub>2</sub> adsorption mechanism of composite PEI@ZIF-8 modified by polyethyleneimine for CO<sub>2</sub>/N<sub>2</sub> separation, *Chem. Eng. J.*, 2015, **280**, 363–369.
- 33 G. Xu, J. Yao, K. Wang, L. He, P. A. Webley, C. S. Chen and H. T. Wang, Preparation of ZIF-8 membranes supported on ceramic hollow fibers from a concentrated synthesis gel, *J. Membr. Sci.*, 2011, **385–386**, 187–193.
- 34 H. Amrouche, S. Aguado, J. Perez-Pellitero, C. Chizallet, F. Siperstein, D. Farrusseng, N. Bats and C. Nieto-Draghi, Experimental and computational study of functionality impact on sodalite-zeolitic imidazolate frameworks for CO<sub>2</sub> separation, *J. Phys. Chem. C*, 2011, **115**, 16425–16432.
- 35 G. Autie-Castro, M. A. Autie, E. Rodríguez-Castellón, C. Aguirre and E. Reguera, Cu-BTC and Fe-BTC metal-organic frameworks: role of the materials structural features on their performance for volatile hydrocarbons separation, *Colloids Surf., A*, 2015, **481**, 351–357.
- 36 C. L. Xin, H. J. Zhan, X. Huang, H. G. Li, N. Zhao, F. K. Xiao, W. Wei and Y. H. Sun, Effect of various alkaline agents on the size and morphology of nano-sized HKUST-1 for CO<sub>2</sub> adsorption, *RSC Adv.*, 2015, **5**, 27901–27911.
- 37 Z. H. Xiang, Z. Hu, D. P. Cao, W. T. Yang, J. M. Lu, B. Y. Han and W. C. Wang, Metal-organic frameworks with incorporated carbon nanotubes: improving carbon dioxide and methane storage capacities by lithium doping, *Angew. Chem., Int. Ed.*, 2011, **50**, 491–494.
- 38 Z. J. Zhang, Y. G. Zhao, Q. H. Gong, Z. Li and J. Li, MOFs for CO<sub>2</sub> capture and separation from flue gas mixtures: the effect of multifunctional sites on their adsorption capacity and selectivity, *Chem. Commun.*, 2013, **49**, 653–661.
- 39 A. Vishnyakov, P. I. Ravikovitch, A. V. Neimark, M. Bülow and Q. M. Wang, Nanopore structure and sorption properties of Cu-BTC metal-organic framework, *Nano Lett.*, 2003, **3**, 713–718.
- 40 S. S. Kaye, A. Dailly, O. M. Yaghi and J. R. Long, Impact of preparation and handling on the hydrogen storage properties of Zn<sub>4</sub>O(1,4-benzenedicarboxylate)<sub>3</sub> (MOF-5), *J. Am. Chem. Soc.*, 2007, **129**, 14176–14177.
- 41 J. I. Langford, Powder pattern programs, *J. Appl. Crystallogr.*, 1971, **4**, 259–260.
- 42 J. I. Langford, The accuracy of cell dimensions determined by Cohen's method of least squares and the systematic indexing of powder data, *J. Appl. Crystallogr.*, 1973, **6**, 190–196.